Catalysis Science & Technology

Accepted Manuscript

ROYAL SOCIETY OF CHEMISTRY

www.rsc.org/catalysis

Catalysis
Science & Technology

RSCPublishing

ARTICLE

Dehydrogenation of Propane over PtSnAl/SBA-15 Catalysts: Al-addition Effect and Coke Formation Analysis

Cite this: DOI: 10.1039/x0xx00000x

Xiaoqiang Fan,[a] Jianmei Li,[†a] Zhen Zhao,[*a] Yuechang Wei,[a] Jian Liu,[*a] Aijun Duan[a] and Guiyuan Jiang[a]

A series of PtSnAl/SBA-15 catalysts were prepared by incipient-wetness impregnation method and their catalytic performances were tested for propane dehydrogenation. The catalysts were characterized by means of XRF, XRD, BET, TEM, UV-Vis DRS, NH_3-TPD, O_2-TPO, ^{27}Al MAS NMR, XPS and in-situ Raman. The addition of aluminum enhances the interaction of Sn-support, and consequently stabilizes the oxidation state of Sn during the propane dehydrogenation reaction. The acid centers formed by aluminium addition show close contact with metal centers (Pt), which favors the synergistic effect of the bifunctional active centers. The high catalytic performance over $PtSnAl_{0.2}$/SBA-15 were obtained, the one pass propane conversion and propene selectivity are 55.9% and 98.5%, respectively. Moreover, the in-situ Raman results indicated the faster coke rate of $PtSnAl_{0.4}$/SBA-15 catalyst than that of $PtSnAl_{0.2}$/SBA-15 catalyst, which may be accelerated by the strong acid due to the excessive aluminum addition.

Received ooth January 2012,
Accepted ooth January 2012

DOI: 10.1039/x0xx00000x

www.rsc.org/

1. Introduction

At present, propylene is typically obtained by means of steam cracking or fluidized catalytic cracking of naphtha. Due to the uncertain oil price and the discoveries in abundance of shale gas in USA, the catalytic dehydrogenation of propane has received much attention as an alternative way for producing propylene. And the chemical reaction equation is $C_3H_8 \rightleftharpoons C_3H_6+H_2$-124 kJ/mol. This reaction is an endothermic process which requires a higher temperature and lower pressure. But high temperature facilitates side reactions of cracking and coke formation. Therefore, many efforts have been made to develop new catalysts with high catalytic properties. The Cr-based catalysts have been widely used for propane dehydrogenation.[1] But the question is the catalyst is typically hazardous. Some other non-noble metal catalysts, including Cu, Fe, etc. have also been investigated.[2,3] But the restriction is their catalytic activity. Pt-based catalysts have been widely investigated for propane dehydrogenation reaction owing to their excellent activity.[4] However, these catalysts usually suffer from the fast deactivation caused by the coke formation and sintering of Pt. There are several strategies to improve the catalytic performance of Pt-based catalyst, including adding a second metal as promoter and selecting suitable support to strengthen the metal-support interaction. The addition of Sn to Pt-based catalyst systems can significantly improve the catalytic activity for the dehydrogenation of propane.[5,6] Usually, the role of Sn is proposed to modify the electronic and geometric properties of Pt.[7,8] Briefly, the formation of heteroatom bonds changes the electronic environment of Pt metal surface, giving rise to the modifications of its electronic structure. The geometry of the bimetallic structure is typically different from that of the parent Pt metals, e.g., the average metal−metal bond lengths change, resulting in the strain effect that is known to modify the electronic structure of the metal through changes in orbital overlap.[9] Furthermore, support effect[10] also influence the catalytic performance of PtSn-based catalysts. Till now, a variety of catalysts, in which PtSn were supported on variable carriers including Al_2O_3, SiO_2, ZSM-5, SAPO-34, Beta,[5,11-13] were studied in order to find an optimum catalyst. Mesoporous siliceous SBA-15 with high surface area, ordered pore structure, and uniform pore size distribution has attracted considerable attention as catalyst support. Shiju et al. have reported that SBA-15 can host both acid and basic sites which can affect the adsorption/desorption regimes of propane/propene.[14] Moreover, SBA-15 unique pore architecture make it very attractive as host for the confinement and stabilization of Pt nanoparticles, which can better maintain their dispersion and catalytic performance even under high reaction temperature conditions.[15] It is reported that Pt-SBA-15 catalyst

show higher selectivity than that of Pt-Al_2O_3 catalyst for propane dehydrogenation due to the lower acidity of Pt-SBA-15 catalyst compared with Pt-Al_2O_3 catalyst. [16,17] Therefore, SBA-15 supported PtSn-based catalyst may be a good candidate for the dehydrogenation of propane.

Although the structure of SBA-15 makes it suitable for being used as the support, the interaction of PtSn with silica framework is weak. Bariås et al.[18] found that the Sn species can be stabilized in the 2+ state on γ-Al_2O_3 but be reduced to metallic Sn and in close contact with Pt (bimetallic clusters) on SiO_2. This change would results in a negative effect on the catalytic activity and causes a large loss of the intrinsic activity. In order to enhance the interaction between metal and support, Al was added to the catalytic system as the form of alumina-modified SBA-15 support, which shows better catalytic performance for propane dehydrogenation.[19] However, compared with SBA-15, alumina-modified SBA-15 shows higher acidity and the reduced surface area and pore volume, which results in the large amount of coke formation and the loss of activity during the propane dehydrogenation. In order to decrease the acidity while maintaining the enhanced interaction between support and metal by Al species, we used the simultaneous impregnation of Pt, Sn and Al precursors to prepare SBA-15-supported PtSnAl catalysts.

In general, as far as the catalysts for the propane dehydrogenation are concerned, deactivation due to coke formation is not avoidable. Li et al.[20] have proposed a mechanism for coke formation based on the kinetic analysis. The reaction between the two strong adsorbed $C_3H_6^*$ was identified as the kinetic relevant step for the coke formation on the Pt surface. And a portion of the precursor migrates to the acid site and is involved in the coke formation on the support. In the present work, Al was added to the catalyst, which will result in the change of the acidity. In order to study the influence of Al addition on coke formation, in-situ Raman experiment was used to characterize the process of coke forming. It is helpful to understand the relationship between the catalyst deactivation and coking.

2. Experimental

2.1 Catalyst preparation

SBA-15 support was synthesized using triblock copolymer (Pluronic P123) as a template according to the procedure reported in the literature.[21] Briefly, 8 g of P123 was dissolved in 240 ml 2M HCl and 60 ml deionized water to form a solution and the solution was stirred for 4 h at 40 °C. Subsequently, 17 g TEOS was gradually added to the solution and continuously stirred for 24 h. The resulting gel was placed into a Teflon autoclave and maintained at 100 °C for 24 h. The solid products were filtered, washed, and dried at 100 °C in air for 12 h, and calcined at 550 °C for 6 h. Finally, mesoporous SBA-15 was obtained.

PtSnAl/SBA-15 catalysts were prepared by incipient-wetness impregnation method. $SnCl_4 \cdot 5H_2O$, $Al(NO_3)_3 \cdot 9H_2O$ and $H_2PtCl_6 \cdot 6H_2O$ precursors were dissolved in deionized water to form a solution and powder SBA-15 was impregnated in the solution. After that, the mixture was sonicated for 30 min and dried at 25 °C for 24 h. The gentle drying of the metal precursor/silica composites after the incipient-wetness impregnation step created favorable conditions to prevent the transport of metal precursors at the external surface during calcination under stagnant air.[22] After being completely dried, the catalysts were calcined at 500 °C for 4 h. The nominal composition of each content was 0.5 wt% Pt; 1 wt% Sn; 0, 0.1, 0.2, 0.3 and 0.4 wt% Al. For the sake of brevity, the catalysts would be named as $PtSnAl_0$/SBA-15, $PtSnAl_{0.1}$/SBA-15, $PtSnAl_{0.2}$/SBA-15, $PtSnAl_{0.3}$/SBA-15, and $PtSnAl_{0.4}$/SBA-15.

2.2 Catalyst characterization

The metallic contents were obtained by XRF measurements on A ZSX 100e XRF spectrometer. Nitrogen adsorption/desorption isotherms at -196 °C were recorded using a Micromeritics TriStar II 3020 porosimetry analyzer. Low-angle XRD patterns were collected in a 2θ range from 0.7 to 10° with a step size of 0.02° on a SIEMENS D5000 diffratometer. Wide-angle XRD patterns were obtained by a powder X-ray diffractometer (Shimadzu XRD 6000) using Cu Kα (λ= 0.15406 nm) radiation. TEM images were taken on JEOL JEM 2100 electron microscope equipped with a field emission source at an acceleration voltage of 200 kV. The UV-Vis DRS experiments were performed on a UV-Vis spectrophotometer (Hitachi U-4100) with the integration sphere diffuse reflectance attachment. XPS were recorded on a Perkin-Elmer PHI-1600 ESCA spectrometer using Mg Kα (hv=1253.6 eV, 1 eV=1.603×10-19 J) X-ray source. The binding energies were calibrated using C1s peak of contaminant carbon (BE = 284.6 eV) as an internal standard. NH_3-TPD was performed in a conventional flow apparatus. O_2-TPO was measured in a conventional flow apparatus. Solid-state ^{27}Al MAS NMR spectra were collected in a Brucker Avance III 400 MHz nuclear magnetic resonance spectrometer. Raman spectra were performed on a Renishaw inVia Reflex Raman spectrometer with a 532 nm laser at room temperature under ambient conditions. The in-situ Raman spectra of the catalyst were collected on a Renishaw inVia Reflex Raman spectrometer with a 532 nm laser. The laser power on the surface of the sample was kept around 1 mW.

2.3 Catalytic activity measurements

The propane dehydrogenation was carried out in a conventional quartz tubular micro-reactor. The catalyst (mass 0.2 g) was placed into the center of the reactor. Before the reaction, the catalyst was reduced with 10% H_2/Ar at 500 °C for 4 h Reaction conditions were as follows: 590 °C for reaction temperature, atmospheric pressure, C_3H_8/Ar=1/5 (molar ratio) and the propane weight hourly space velocity (WHSV) is 2.5 h^{-1}. The reaction products were analyzed with an online SP-2100 gas chromatography. An aluminum column was used for the separation of CH_4, C_2H_4, C_2H_6, C_3H_6, and C_3H_8. The conversion of propane and selectivity of propene were defined as follows:

$$\text{Conversion of propane (\%)}=\frac{\text{Content of propane in feedstock - content of propane in product}}{\text{Content of propane in feedwork}}\times 100$$

$$\text{Selectivity to propene (\%)}=\frac{\text{Content of propene in product}}{\text{Content of propane in feedstock - content of propane in product}}\times 100$$

3. Results

3.1. Physicochemical properties of catalysts

3.1.1 The results of XRF and XRD

The contents of Pt, Sn and Al elements were determined by XRF and the results are present in Table 1. All the metallic ions were successfully loaded on SBA-15 support by the simultaneous impregnation method. The low-angle XRD patterns of the SBA-15 and PtSnAl/SBA-15 samples are shown in Fig. 1A. The XRD pattern of SBA-15 exhibits a sharp peak at about 0.92° together with two additional weak peaks, corresponding to the (100), (110), and (200) planes, which are the characteristics to highly ordered hexagonal 2D structures of

P6mm symmetry.[21] After loading Pt, Sn and Al, all the patterns of PtSnAl/SBA-15 show these three peaks with high intensity, indicating the hexagonal mesostructure is intact after loading metal. The corresponding lattice spacings (d_{100}) and unit-cell parameters (a_0) are listed in Table 1. It can be observed that the d_{100} spacing after loading Pt, Sn and Al are quite similar to SBA-15, indicating no significant alteration symmetry of pore structure of PtSnAl/SBA-15. Accordingly, for low metal concentration, the mesoporous structure of SBA-15 support accommodates the nanoparticles in the inner channels and does not alter the diffraction peaks.[23,24]

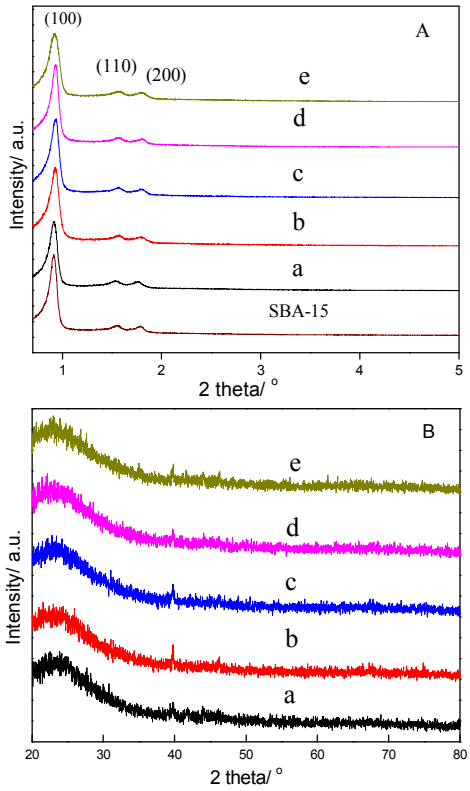

Fig. 1 (A) Low-angle and (B) wide-angle XRD patterns of SBA-15 and PtSnAl/SBA-15 catalysts: (a) $PtSnAl_0$/SBA-15, (b) $PtSnAl_{0.1}$/SBA-15, (c) $PtSnAl_{0.2}$/SBA-15, (d) $PtSnAl_{0.3}$/SBA-15, (e) $PtSnAl_{0.4}$/SBA-15.

Table 1 Chemical and structural properties of PtSnAl/SBA-15 material

Sanmple	Pt[a] (wt%)	Sn (wt%)[a]	Al[a] (wt%)	d_{100}[b] (nm)	a_0[c] (nm)
SBA-15				9.5	11.0
$PtSnAl_0$/SBA-15	0.43	0.78		9.5	11.0
$PtSnAl_{0.1}$/SBA-15	0.45	0.81	0.10	9.5	11.0
$PtSnAl_{0.2}$/SBA-15	0.44	0.79	0.19	9.6	11.1
$PtSnAl_{0.3}$/SBA-15	0.44	0.78	0.28	9.6	11.1
$PtSnAl_{0.4}$/SBA-15	0.45	0.80	0.39	9.5	11.0

[a] The metallic contents measured by XRF.
[b] d_{100} is the lattice spacing obtained by low angle XRD.
[c] a_0 is the hexagonal unit-cell parameter calculated using the equation: $a_0 = 2d_{100}/\sqrt{3}$.

XRD patterns recorded in the wide-angle domain for these materials are depicted in Fig. 1B. All the patterns show broad maxima at 2θ of 23.5° which is typical peak of amorphous silica.[25] Besides the characteristic patterns of SBA-15, the XRD reflections at 2θ of 39.8°, 46.2°, 67.4° and 81.4° can be attributed to (111), (200), (220) and (311) inter planar spacings of the cubic Pt metal structure, respectively.[26] The presence of Pt was confirmed by XRD patterns, but there are no obviously XRD diffractions from M or MO_x (M=Sn, Al). The absence of these XRD diffractions for PtSnAl/SBA-15 catalysts is probably due to the high dispersion of M or the formation of amorphous MO_x phases.

3.1.2. The results of Nitrogen-adsorption

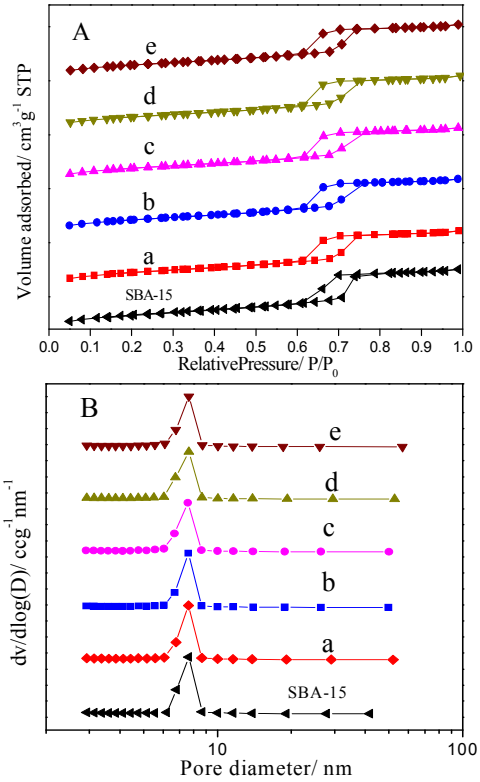

Fig. 2 (A) N_2 adsorption-desorption isotherms and (B) pore size distribution of SBA-15 and PtSnAl/SBA-15 catalysts: (a) $PtSnAl_0$/SBA-15, (b) $PtSnAl_{0.1}$/SBA-15, (c) $PtSnAl_{0.2}$/SBA-15, (d) $PtSnAl_{0.3}$/SBA-15, (e) $PtSnAl_{0.4}$/SBA-15.

Table 2 Textural properties of SBA-15 and supported PtSnAl/SBA-15 catalysts

sample	S_{BET}[a] ($m^2 \cdot g^{-1}$)	V_t[b] ($cm^3 \cdot g^{-1}$)	Vmes[c] ($cm^3 \cdot g^{-1}$)	V_{mic}[d] ($cm^3 \cdot g^{-1}$)	BJH[e] (nm)
SBA-15	857	1.03	0.93	0.064	7.7
$PtSnAl_0$/SBA-15	791	0.94	0.84	0.062	7.7
$PtSnAl_{0.1}$/SBA-15	777	0.93	0.82	0.060	7.6
$PtSnAl_{0.2}$/SBA-15	766	0.92	0.82	0.058	7.6
$PtSnAl_{0.3}$/SBA-15	754	0.91	0.81	0.056	7.7
$PtSnAl_{0.4}$/SBA-15	746	0.90	0.81	0.055	7.6

[a] Calculated by the BET method.
[b] The total pore volume was obtained at a relative pressure of 0.98.
[c] The mesoporous volume was calculated using the BJH method.
[d] The microporous volume was calculated using the t-plot method.

[e] Mesopore diameter was calculated using the BJH method.

The textural properties of the calcined catalysts were investigated by nitrogen adsorption-desorption and the corresponding isotherms and pore size distributions are shown in Fig. 2. As shown in Fig. 2A, SBA-15 exhibits isotherm of type IV with hysteresis loops of type H1. It indicates that the highly ordered mesoporous SBA-15 solids have a narrow pore size distribution of the cylindrical channels, which is in good agreement with the results obtained by low-angle XRD. Likewise, it is noticed that PtSnAl/SBA-15 samples display isotherms very similar in shape to that of SBA-15, which are characterized by steep adsorption/desorption branches and uniform H1 hysteresis loops at relative pressures (P/P_0) of 0.6-0.8, indicating that these catalysts retain the initial texture of the SBA-15. The pore size distribution curve shown in Fig. 2B display pore size with high uniformity and show that the pore size nearly keep unchanged, which may be caused by low metal loading and indicates the highly dispersion of the metal.

On the basis of the adsorption/desorption isotherms, the textural properties of SBA-15 and PtSnAl/SBA-15 catalysts were calculated by specific algorithms and they are shown in Table 2. Compared with SBA-15, the BET surface area of $PtSnAl_0$/SBA-15 catalyst decreases from 857 $m^2 \cdot g^{-1}$ to 791 $m^2 \cdot g^{-1}$ after loading of Pt and Sn, and it further decreases with the increasing loading amount of Al. Meanwhile, the total pore volume and mesopore volume decrease from 1.03 and 0.93 $cm^3 \cdot g^{-1}$ to 0.90 and 0.81 $cm^3 \cdot g^{-1}$, respectively, with the increasing of metal loading amount. It indicates that the metals are dispersed in the mesopores of the SBA-15, as reported the noble metal nanoparticles confined in the mesopores of SBA-15.[27]

3.1.3The results of TEM

To further investigate the morphology of nanoparticles and to provide evidence on their distribution, TEM analyses were carried out. Fig. 3 shows the TEM images of (a) $PtSnAl_0$/SBA-15, (b) $PtSnAl_{0.2}$/SBA-15 and (c) $PtSnAl_{0.4}$/SBA-15 catalysts. All samples exhibit highly ordered mesoporous SBA-15 structure composed of cylindrical mesochannels with a narrow size distribution, which is in good agreement with the results of N_2 physisorption. Meanwhile, no large aggregates of the metals on the external surface of SBA-15 were observed. The nanoparticles are well dispersed and uniformly distributed throughout the pores of SBA-15 under the form of rodlike particles with a diameter of ~8 nm (consistent with the pore diameter of the SBA-15) and variable lengths between 10 and 50 nm. Some nanorods have grown in adjacent mesopores forming nanobundle-like agglomerates. This confirms that the formation of highly dispersed metal nanoparticles confined within the channels of SBA-15. The confined effect of SBA-15 has been proved to stabilize the nanoparticles and thus inhibits the sintering of nanoparticles,[28] which can improve the stability of the catalysts during the propane dehydrogenation reaction.

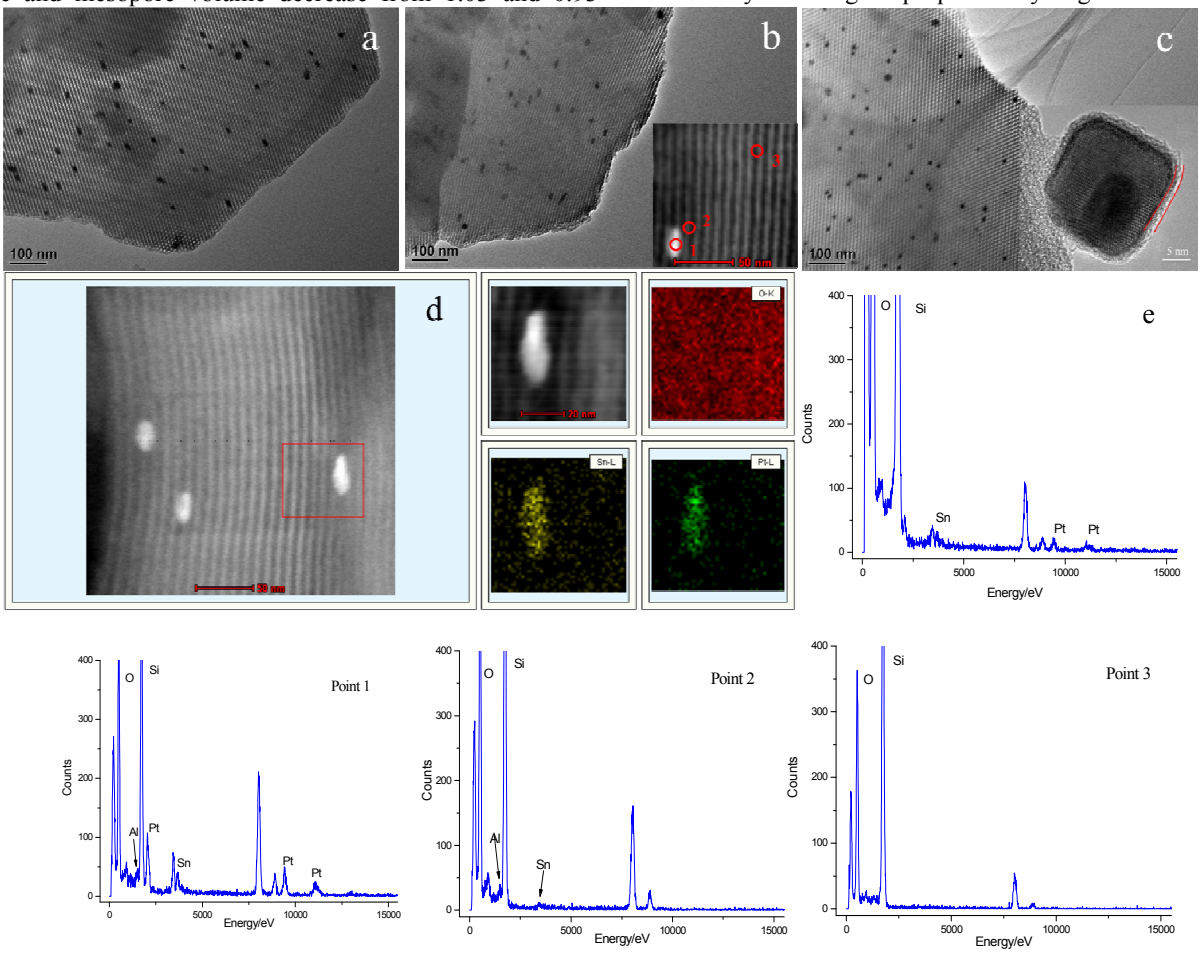

Fig. 3 TEM images of (a) $PtSnAl_0$/SBA-15, (b) $PtSnAl_{0.2}$/SBA-15 and (c) $PtSnAl_{0.4}$/SBA-15 catalysts; (d) and (e) HAADF-STEM image and EDS elemental mapping of $PtSnAl_0$/SBA-15. (Inset of (b) is HAADF-STEM image of $PtSnAl_{0.2}$/SBA-15; Inset of (c) is HRTEM image of $PtSnAl_{0.4}$/SBA-15)

The inset of Fig. 3c shows the HRTEM of the nanoparticle in $PtSnAl_{0.4}$/SBA-15 catalyst. It can be seen that the surface of the nanoparticle shows the existence of amorphous phase, indicating the presence of SnO_x and Al_2O_3 phase in the surface of Pt nanoparticle. Distributions of Pt and Sn on $PtSnAl_0$/SBA-15 catalyst were confirmed by means of HAADF-STEM experiment combined with EDS element-mapping analysis. Fig. 3d shows the HAADF-STEM image of $PtSnAl_0$/SBA-15 catalyst together with the elemental mapping images of O, Sn and Pt in the same region. It is clear that the nanoparticle is confined in the mesopore from the HAADF-STEM image. In the element-mapping images, the Pt and Sn signals show similar distributions, which coincides with the bright contrast in HAADF image. The simultaneous presence of Pt and Sn in one nanoparticle indicates the existence of strong interactions between Pt and Sn.

In order to investigate the distribution of Pt, Sn and Al on PtSnAl/SBA-15 catalysts, EDX analysis in the spot mode was carried out. The inset of Fig. 3b shows the HAADF image of $PtSnAl_{0.2}$/SBA-15 catalyst and the EDX spectra from the nanoparticles (point 1), support near the nanoparticles (point 2) and the support far away from the nanoparticles (point 3) were also shown in Fig. 3. The elemental composition of the nanoparticles (point 1) indicates the presence of Pt, Sn and Al, while the peak intensity of Al is weaker than that of Sn and Pt. Point 2 shows the presence of Al and trace amount of Sn in the support near the nanoparticles, indicating that most of Al species and fraction of Sn species are interaction with the support. Point 3 shows only the presence of Si and O. It indicates that the elements of Pt, Sn and Al are not in the form of evenly dispersed in the whole surface of the support. Pt, Sn and Al are present in the form of the nanoparticles in the mesopores, while some Sn and most of Al exist in the support near the nanoparticles.

3.1.4 The results of 27Al MAS NMR

^{27}Al MAS NMR spectroscopy is known as an efficient probe to determine the coordination and local structure of specific aluminum species in zeolite materials. To further investigate the nature of Al species over PtSnAl/SBA-15 catalysts, ^{27}Al MAS NMR experiments were carried out and the spectra are shown in Fig. 4. For the Al-containing mesoporous materials, the peak at 54 ppm is assigned to Al in a tetrahedral environment (structural unit AlO_4) and the peak at 0 ppm is related to octahedral Al (structural unit AlO_6).[29] As shown in Fig. 4, both tetrahedral and octahedral Al structure units are existent. The higher intensity of tetrahedral Al in PtSnAl/SBA-15 catalysts indicates that a majority of Al incorporate into the tetrahedral framework of SBA-15, which is consistent with the EDS result.

According to the EDS and ^{27}Al MAS NMR results, most of Al species are existent in the framework of SBA-15 near the metal active site. It results in a close contact of Al species and PtSn active sites. The close contact of Al with PtSn and support may be beneficial to a stronger interaction yielded by the simultaneous impregnation.[30]

3.1.5 The results of XPS

X-ray photoelectron spectroscopy studies were conducted on the reduced PtSnAl/SBA-15 catalysts to determine the chemical states from their corresponding binding energies. Fig. 5A shows the XPS spectra corresponding to the Sn $3d_{5/2}$ level of the reduced PtSnAl/SBA-15 catalysts. The FWHM of these spectra is of ~3 eV indicating the presence of multiple species.[31] The deconvolution of the spectra yielded four peaks positioned at 485.4, 486.3, 487.3 and 488.6 eV, representative of the different types of tin species. The Sn $3d_{5/2}$ at 485.4 eV is assigned to Sn^0 in the Pt-Sn alloy. The peaks at 486.3 and 487.3 eV are corresponded to oxidized Sn i.e. Sn^{2+} and Sn^{4+}, respectively. And the peak at 488.6 eV is attributed to Sn species bound to the support,[32] which is demonstrated by the EDS result that the existence of Sn in SBA-15 support. The quantitative analysis results for XPS are shown in Table 3. The most of Sn species are characteristic of oxidized Sn. What's more, the content of Sn^0 species at $PtSnAl_0$/SBA-15 catalyst is 17.3 %, while it decreases to 13.5 % at $PtSnAl_{0.1}$/SBA-15 catalyst. The gradually decreasing with the increasing of Al in PtSnAl/SBA-15 catalysts indicates that the presence of Al inhibits the reduction of Sn species to Sn^0. It is because that the stronger interaction of Sn and Al stabilizes the oxidized tin species and hinders the reduction of SnO_x than that of tin and silicon.[33] The atomic ratios of Sn/Pt at PtSnAl/SBA-15 catalysts from XPS results are shown in Table 3. The Sn/Pt ratios in these catalysts are much higher than 3.4 (calculated from the Pt and Sn precursors), indicating the enrichment of Sn species on the surface of Pt nanoparticles. The segregation of Sn at the surfaces of the bimetallic PtSn particle systems has been widely observed in the previous studies.[34] In the present work, the surface segregation could be interpreted by the different redox potentials between two metals. And comparing with Pt atom, Sn atom shows higher surface mobility and lower surface energy, which results in the migration of Sn to the particle surface.[35] Meanwhile, the surface Sn atoms will be oxidized due to their low coordination number.[36] As shown in Table 3, the ratios of Sn/Pt decrease from 10.0 to 6.8 with the increasing of Al content from 0 to 0.4, which may be due to the formation of amorphous Al_2O_3 on the surface of the nanoparticle.

Fig. 5B shows the Sn $3d_{5/2}$ XPS spectra of the PtSnAl/SBA-15 catalysts after propane dehydrogenation reaction. A slight shift to low binding energy is displayed from $PtSnAl_{0.4}$/SBA-15 to $PtSnAl_0$/SBA-15 catalyst. It has been reported that alloying with Pt might cause the shift.[35,37] It is indicated that Sn species was reduced during the reaction and alloyed with Pt. Moreover, alloying degree increased with the decreasing of Al content. After deconvolution of these spectra, the proportion of peaks at 485.4 and 486.3 eV is greater than that before reaction and the tendency increases with decreasing of Al loading amount, indicating the addition of Al inhibits the reduction of Sn species during the propane dehydrogenation.

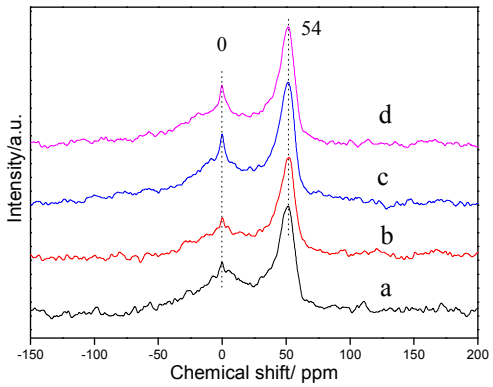

Fig. 4 ^{27}Al MAS NMR spectra of PtSnAl/SBA-15 catalysts: (a) $PtSnAl_{0.1}$/SBA-15, (b) $PtSnAl_{0.2}$/SBA-15, (c) $PtSnAl_{0.3}$/SBA-15, (d) $PtSnAl_{0.4}$/SBA-15.

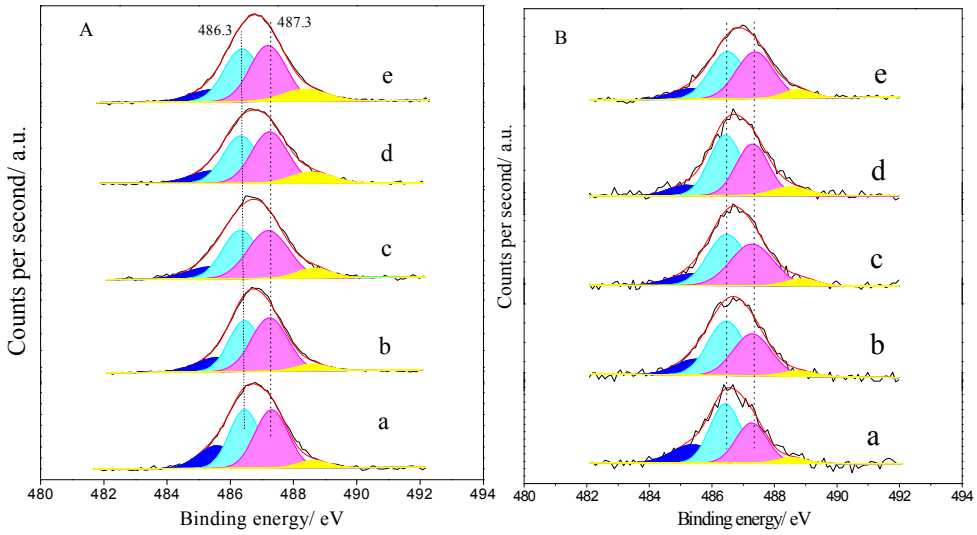

Fig. 5 XPS spectra corresponding to $Sn3d_{5/2}$ on reduced PtSnAl/SBA-15 catalysts (A) before reaction and (B) after reaction: (a) $PtSnAl_0$/SBA-15, (b) $PtSnAl_{0.1}$/SBA-15, (c) $PtSnAl_{0.2}$/SBA-15, (d) $PtSnAl_{0.3}$/SBA-15, (e) $PtSnAl_{0.4}$/SBA-15.

Table 3 XPS spectra $Sn3d_{5/2}$ peak analysis and Raman spectra analysis results for PtSnAl/SBA-15

Sample	Sn species (%)		Sn/Pt	I_D/I_G
	Sn^0	Sn^{2+},Sn^{4+}		
$PtSnAl_0$/SBA-15	17.3	82.7	10	1
$PtSnAl_{0.1}$/SBA-15	13.5	86.5	8.1	0.62
$PtSnAl_{0.2}$/SBA-15	12.4	87.6	7.6	0.62
$PtSnAl_{0.3}$/SBA-15	11.9	88.1	7.5	0.43
$PtSnAl_{0.4}$/SBA-15	10.8	89.2	6.8	0.39

3.1.6 The results of UV-Vis DRS

UV-Vis DRS is a sensitive and convenient tool, which is widely used to detect the coordination states of the transition metal ions in zeolites particularly in the case of Ti, Sn, or Zr-containing metallosilicates. Fig. 6 shows the UV-Vis absorption spectra of PtSnAl/SBA-15 catalysts. For the $PtSnAl_0$/SBA-15 catalyst, there are two adsorption bands with maximum intensities at 215 and 258 nm. According to the literature on Sn isomorphously substituted SBA-15,[38] the O→Sn LMCTs in tetrahedral (T_d) and octahedral (O_h) environments appear at around 205 and 230 nm, respectively, while the hexacoordinated Sn-O-Sn type species appear at around 280 nm. In the present study, the band at 215 nm is assigned to the O→Sn LMCTs in T_d coordination, which implies that some Sn species substitute Si in the framework position. The band at 258 nm corresponds to the band gap transition of amorphous Sn oxide. And the blue-shift of this band is due to the quantum size effect. After addition of Al, there is another peak at 244 nm, which is assigned to the O→Sn LMCTs in O_h coordination, and the intensity of this absorption band increases with the increasing of Al content. The suggested model for the coordination states of Sn is shown in Fig. S1. The appearance of the O→Sn LMCTs in O_h coordination and the decrease of the O→Sn LMCTs in T_d coordination implies that some of Sn in the silica framework migrate out and aggregate on the surface of silica wall by bridged oxygen atoms with the increase of Al content. The increase of this coordination state Sn may be favorable for enhancing the interaction between SBA-15 support and Pt by the surface Si–O–Sn or Al–O–Sn species. Moreover, the intensity of 258 nm band decreases with increasing Al amount, suggesting the decrease of SnO_2 agglomerates and high dispersion of Sn species.

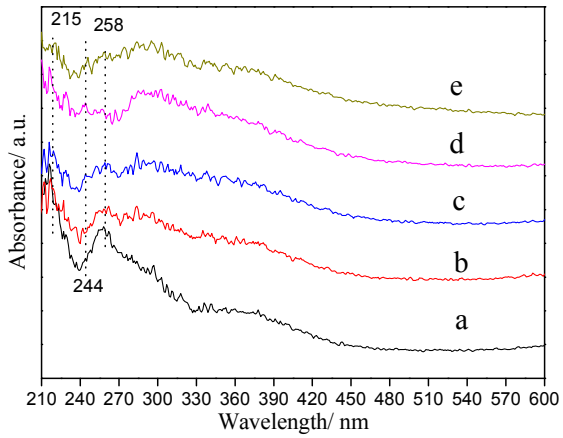

Fig. 6 UV-Vis diffuse reflectance spectra of PtSnAl/SBA-15 catalysts: (a) $PtSnAl_0$/SBA-15, (b) $PtSnAl_{0.1}$/SBA-15, (c) $PtSnAl_{0.2}$/SBA-15, (d) $PtSnAl_{0.3}$/SBA-15, (e) $PtSnAl_{0.4}$/SBA-15.

The results of UV-Vis DRS indicate that the Sn species exist in the form of oxidized Sn in PtSnAl/SBA-15 catalysts, which is consistent with the XPS results. The addition of Al, on the one hand, promotes the transformation of T_d coordination Sn to O_h

coordination Sn, which is in favor of the interaction with Pt and the support. On the other hand, it decreases the amount of hexacoordination SnO_2 agglomerates and increases the surface O_h coordination Sn species, which is more stable by connecting with Si through bridged oxygen.

3.1.7 The results of NH_3-TPD

To investigate the influence of addition Al on the acidity of PtSnAl/SBA-15 catalysts, the NH_3-TPD analyses were carried out. As shown in Fig. 7, the NH_3-TPD profile of pure silica SBA-15 shows no evident peak, indicating its negligible acidity. An interesting phenomenon takes place in the NH_3-TPD result of $PtSnAl_0$/SBA-15, where the desorption of NH_3 in 150-350 ^oC happens. This indicates that the generation of the weak acid sites. It has been reported that two types of Lewis acid sites are shown to exist in Sn-silica material due to the incorporation of Sn into the silica framework and formation of $Sn(–Si–O–)_4$ (site A) and $Sn(–Si–O–)_3Sn–OH$ (site B) sites.[39] Fig. S1 shows the suggested model of the acid site. The generation of desorption peak at 150-350 ^oC in $PtSnAl_0$/SBA-15 catalysts is corresponded to the Lewis acid sites due to the incorporation of Sn in SBA-15 as demonstrated in UV-Vis DRS results. Although the surface Sn (site B) or framework Sn (site A) can not be distinguished according to the NH_3-TPD and UV-Vis results, it can been speculated that the adding of Al promotes the transformation of framework Sn to surface Sn which is more active.[39]

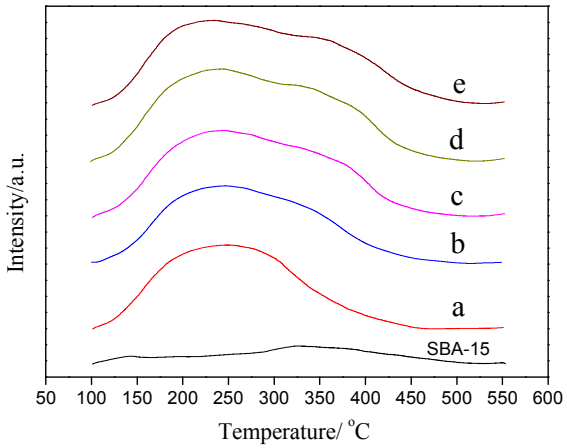

Fig. 7 NH_3-TPD profiles of SBA-15 and PtSnAl/SBA-15 catalysts: (a) $PtSnAl_0$/SBA-15, (b) $PtSnAl_{0.1}$/SBA-15, (c) $PtSnAl_{0.2}$/SBA-15, (d) $PtSnAl_{0.3}$/SBA-15, (e) $PtSnAl_{0.4}$/SBA-15.

According to the ^{27}Al NMR result, most of Al species in PtSnAl/SBA-15 catalysts were existent in the form of framework AlO_4. Whenever an Al^{3+} cation replaces a Si^{4+} cation, an additional proton (H^+) is required to maintain electrical neutrality. These additional protons provide the catalyst Brønsted acid sites.[41] As shown in Fig. 7, the incorporation of Al into framework of SBA-15 leads to the generation of the desorption peak at about 400 ^oC, which is attributed to the Brønsted acid sites. And with increasing of Al content, the amount of desorbed NH_3 at about 400 ^oC increases, indicating the augment of Brønsted acid sites, which results in the increase of acidity of the catalyst. The aicd type and strength will influence the catalytic performance.[42]

As mentioned above that the most of Al incorporate into the framework of SBA-15 to form Brønsted acid sites, which distributes around the metal active center. The local distribution of Al generates the local acid centers and show close contact with the metal centers. The close contact of Pt and Brønsted acid sites may result in the electron transfer happened from Pt to Brønsted proton.[43] It can decreases the electron transfers to Sn^{n+}, and then prevents the formation of metallic Sn from SnO_x, which can refrain the deactivation of the catalysts. A highly stable state of Sn is more difficultly reduced during dehydrogenation at high reaction temperature, which is favorable for the catalytic stability.

3.2 Catalytic performance for propane dehydrogenation

PtSnAl/SBA-15 catalysts were tested for propane dehydrogenation. Fig. 8 exhibits the catalytic performances of the different catalysts. For $PtSnAl_0$/SBA-15 catalyst, the initial propane conversion is 50.8% and after 6 h reaction it becomes 35.3%. For $PtSnAl_{0.1}$/SBA-15 and $PtSnAl_{0.2}$/SBA-15 catalysts, the propane conversion increases to 55.1% and 55.9%, respectively. Meanwhile, the catalytic stabilities of these catalysts are as good as that of $PtSnAl_0$/SBA-15 catalyst, which shows the final propane conversion of 38.8 ($PtSnAl_{0.1}$/SBA-15) and 40.5% ($PtSnAl_{0.2}$/SBA-15), respectively. Furthermore, there are significant differences among the PtSnAl/SBA-15 catalysts for the propane conversion and catalytic stability. The $PtSnAl_{0.1}$/SBA-15 and $PtSnAl_{0.2}$/SBA-15 catalysts show higher initial and final conversion of propane than that of $PtSnAl_0$/SBA-15. And $PtSnAl_{0.2}$/SBA-15 catalyst shows the best catalytic performance on propane dehydrogenation in our experiments. Compared with $PtSnAl_0$/SBA-15 catalysts, the promotion effect on the catalytic performance over PtSnAl/SBA-15 catalysts may be related to the stabilized effect of Sn species by the addition of Al, since the presence of Si in the support cannot stabilize the Sn species. Therefore, appropriate amount of Al should be added to the catalyst system to maintain the oxidative state of Sn.

However, for $PtSnAl_{0.3}$/SBA-15 and $PtSnAl_{0.4}$/SBA-15 catalysts, the initial propane conversions (48.4% for $PtSnAl_{0.3}$/SBA-15 and 43.4% for $PtSnAl_{0.4}$/SBA-15) are lower than that of $PtSnAl_0$/SBA-15 catalyst. It may be due to that the part of the metal active centers was covered by Al_2O_3 species during the simultaneous impregnation, which is demonstrated by the TEM results. And these two catalysts show more quickly deactivation, which may be caused by the change of the acidity during the adding of Al. Moreover, as shown in Fig. 8B, the selectivity of propene on these catalysts shows similar trends with $PtSnAl_0$/SBA-15 catalyst during the reaction procedure. Table S1 in supporting information lists some related literature on different catalysts for propane dehydrogenation. It can be seen that compared with the non-noble catalysts, the noble (Pt) catalysts show higher catalytic performance for propane dehydrogenation. Despite differences in catalyst compositions and reaction conditions, PtSnAl/SBA-15 catalyst used in this study shows better catalytic performance than most of the catalysts. Compared with the silica-based catalysts, the promotion effect on the catalytic performance over PtSnAl/SBA-15 catalysts may be related to the stabilized effect of Sn species by the addition of Al, since the presence of Si in the support cannot stabilize the Sn species. Therefore, appropriate amount of Al should be added to the catalytic system to maintain the oxidation state of Sn.

To further investigate the influence of addition Al on the catalytic performance, a comparison of the $PtSnAl_0$/SBA-15 and $PtnAl_{0.2}$/SBA-15 catalysts by using a cycle reaction is made and the results are shown in Fig. S2. It is obvious that despite the gradual deactivation, the conversion of propane during the

cycles is always higher for $PtSnAl_{0.2}$/SBA-15 catalyst than for the $PtSnAl_0$/SBA-15 catalyst. The deactivation rate of $PtSnAl_0$/SBA-15 catalyst is faster than that of $PtSnAl_{0.2}$/SBA-15 after regeneration. These results indicate that the $PtSnAl_{0.2}$/SBA-15 catalyst shows higher stability than PtSnAl/SBA-15 catalyst in the propane dehydrogenation reaction.

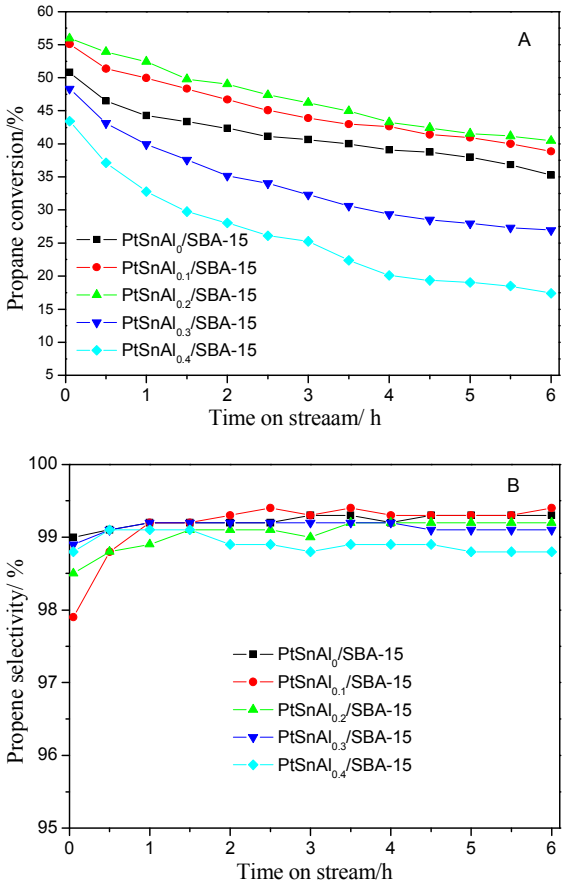

Fig. 8 (A) Propane conversion and (B) propene selectivity over PtSnAl/SBA-15 catalysts. Reaction conditions: 590 °C, C_3H_8:Ar=1:5, WHSV of propane=2.5 h^{-1}.

4 Discussion

4.1 The Effect of Al Addition on the Structure of PtSnAl/SBA-15 Catalysts

The structure of catalyst has influence on the catalytic performance. In order to investigate the influence of Al addition on the catalytic performance, the structure influence induced by Al is discussed firstly. For $PtSnAl_0$/SBA-15 catalyst, the TEM results (Fig. 3d) show that the nanoparticles are confined in the mesopores of SBA-15 and consist of Pt and Sn. And according to XPS spectra, the atomic ratio of Sn/Pt was 11, whereas EDS result suggested a ratio of around 1.9 (Fig. 3e), which confirms that Sn is enriched on the surface of the nanoparticle. And the most of Sn species are existent in the form of oxidation state according to XPS and UV-Vis DRS results. Therefore, based on the structural characterization results, the nanoparticles of $PtSnAl_0$/SBA-15 catalyst in mesopores may be existent in the form of a surface architecture consisting of Pt nanoparticle decorated by surface SnO_x. Nevertheless, the structure may not be stable during the reaction due to the SnO_x phase are often metastable,[44] and some structural changes often occur attributing to the different temperature and reaction atmosphere.[45] After the reaction, SnO_x species was reduced and alloyed with Pt. This process usually results in the deactivation during propane dehydrogenation.[46] Therefore, the addition of Al to PtSn/SBA-15 system has been used as a binder to strengthen the interaction of Pt–SnO_x, and PtSn–support. According to the XPS and UV-Vis results, the addition of Al dramatically restrains the formation of Sn^0 by enhancing the interaction of SBA-15 and Sn through surface Si–O–Sn or Al–O–Sn, and promotes the transformation of framework Sn(–Si–O–)$_4$ to surface Si–O–Sn–OH or Al–O–Sn–OH. Meanwhile, the tetrahedral Al in the framework of SBA-15 possess strong interaction with SBA-15 support by Si–O–Al, thus stabilizing the Pt particles.

4.2 The Effect of Al Addition on Physico-chemical Properties and Catalytic Performance

Density functional theory calculations for propane dehydrogenation show that a weaker adsorption of propene on PtSn than on Pt. It is due to that Sn donates electrons to Pt and results in a lower d-band center of Pt atom on PtSn.[47,48] The weakening of propene adsorption promotes its desorption and therefore enhances the selectivity of propene.[49] In real PtSn-based catalysts, it can be deduced that the surface decorated SnO_x decreases adsorption of propene, which is favorable for propane dehydrogenation reaction. The high catalytic performance of $PtSnAl_0$/SBA-15 catalyst may be due to the efficient decoration of Pt by surface SnO_x. The confined effect of PtSn nanoparticles in the mesopores inhibits the sintering of Pt, which is favorable for maintaining the high stability of the catalyst.

For the $PtSnAl_0$/SBA-15 catalysts, the active site is mainly supplied by noble metal. After adding Al on this system, the acid sites formed and increased with the increasing of Al content. Therefore, the PtSnAl/SBA-15 catalysts act as bifunctional catalysts for propane dehydrogenation as described in other reports.[50] The rule of acid sites is usually the isomerization through the carbenium ion intermediates.[51] Meanwhile, propane can also dehydrogenation through another path: hydride transfer from propane to carbenium ions followed by propene desorption.[52] As far as the metal catalysis is concerned, according to the above results, it may be deduced that the Pt atom interacts with a Brønsted proton after adding Al. The electron transfer between Pt and support results in an electron redistribution in Pt atom, which may lead to some decoration on electronic structure.[41] The enhanced catalytic performance may be partly from the decorating of the Pt electronic structure and the synergistic effect of the bifunctional active centers. For the $PtSnAl_{0.2}$/SBA-15 catalyst, the best match of the noble metal active centers and acid centers generate the enhanced catalytic performance for propane dehydrogenation.

Moreover, based on the XPS results after reaction, the addition of Al inhibits the reduction of Sn species by enhancing the interaction of SBA-15 and Sn through surface Si–O–Sn or Al–O–Sn. Thus, the catalyst keeps oxidative state of Sn species after the reaction. And it slows down the deactivation of the catalyst during the propane dehydrogenation cycles.

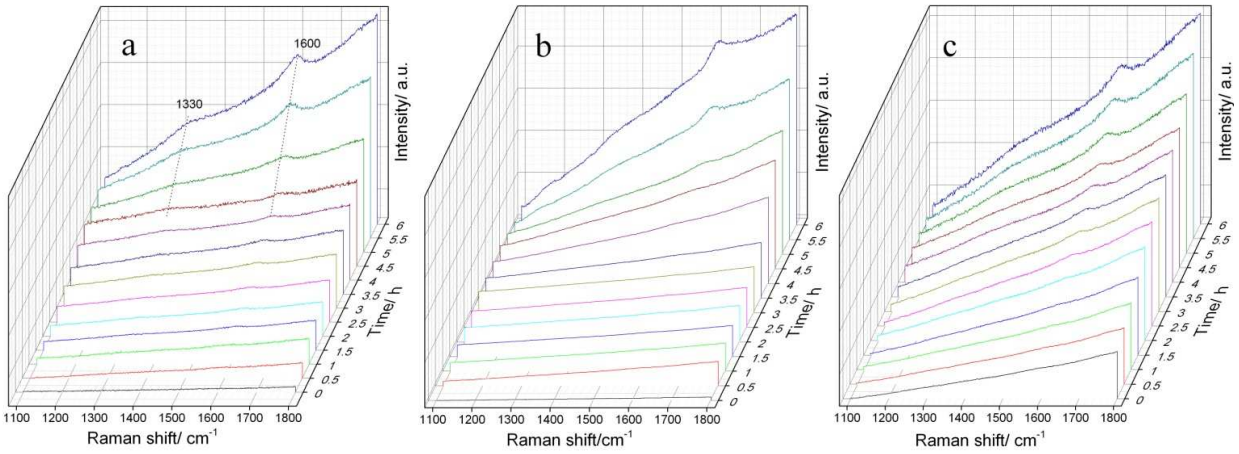

Fig. 9 In-situ Raman spectra of (a) $PtSnAl_0$/SBA-15, (b) $PtSnAl_{0.2}$/SBA-15 and (c) $PtSnAl_{0.4}$/SBA-15 catalysts during the process of propane dehydrogenation.

4.3 Coke Analysis

For PtSnAl/SBA-15 catalysts, different Al loading results in the different acid amount and acid strength, which may lead to different coke formation rate. The formation rate of coke on these catalysts influences the propane dehydrogenation deactivation rate. In this work, in-situ Raman spectra was used to investigate the formation of coke.[53,54] Fig. 9 shows the in-situ Raman spectra of (a) $PtSnAl_0$/SBA-15, (b) $PtSnAl_{0.2}$/SBA-15 and (c) $PtSnAl_{0.4}$/SBA-15 catalysts for propane dehydrogenation. As shown in Fig. 9a, there is no apparent peak at the beginning of the reaction on $PtSnAl_0$/SBA-15 catalyst. After about 4.5 h, two Raman bands at around 1600 and 1330 cm^{-1} were observed and increased with increasing of the reaction time. The band at 1600 cm^{-1} is called G band, which is actually the stretching vibration of any pair of sp^2 sites, whether in C=C chains or in aromatic rings. The band at 1330 cm^{-1} is ascribed to D band or disordered band which is the breathing mode of those sp^2 sites only in rings, not in chains.[55] Therefore, these bands provided information not only on the amount of coke formed on the catalyst, but also on its nature. As shown in Fig. 9a, the Raman bands at around 1330 and 1600 cm^{-1} revealed that carbon deposition on $PtSnAl_0$/SBA-15 catalyst took place after about 4.5 h reaction. And its intensity increases with the further reaction. The $PtSnAl_{0.2}$/SBA-15 shows similar coke formation rate to PtSn/SBA-15 catalyst, indicating that a small amount of aluminum in this system does not accelerate the coke formation. However, compared with these two catalysts, $PtSnAl_{0.4}$/SBA-15 catalyst shows fast coke formation, which is demonstrated by the early appearance of Raman bands after 3 h reaction. In the presence of acid sites, propene oligomerization, oligomei cyclization, etc. happened and coke forms. The higher acid sties generally promote these procedure and result in a quick coke formation rate. For $PtSnAl_{0.4}$/SBA-15 with large acid amount and acid strength, hydrogenolysis and coke reaction can be carried out easily. In order to avoid the strong fluorescence phenomenon during in-situ Raman experiment, the normal Raman spectra for PtSnAl/SBA-15 catalysts after 6 h reaction were collected. The spectra are shown in Fig. 10 and the intensity ratio of D and G band (I_D/I_G) are listed in Table 3. As shown in Fig. 10, the stronger peak intensity of the spectra are depicted, which due to the lower fluorescence and different testing atmosphere. The I_D/I_G of different PtSnAl/SBA-15 catalysts decreases with increasing of Al amount. This indicates that the nature of coke becomes more graphitic and lower ratio of H/C with increasing Al content. The reason is that the propene would initially form oligomers (or polymers) and aromatics, and these surface species would lose hydrogen and become more graphitic with the increasing of acidity.[56] In this system, the strong acid site was introduced by excessive Al addition and the acidity of the support can promote the cracking/isomerization reaction,[9] which results in the fast formation of coke for $PtSnAl_{0.4}$/SBA-15 catalyst.

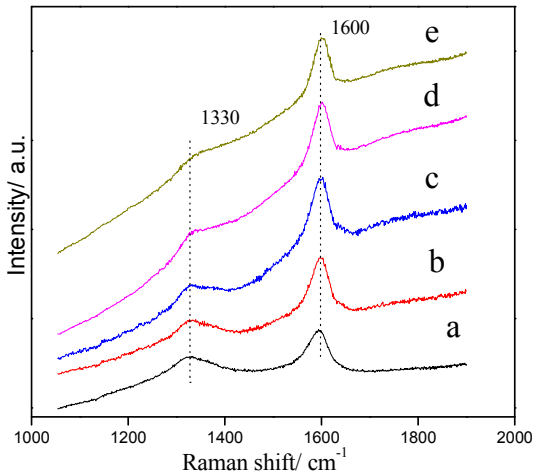

Fig. 10 Raman spectra of the coked catalysts: (a) $PtSnAl_0$/SBA-15, (b) $PtSnAl_{0.1}$/SBA-15, (c) $PtSnAl_{0.2}$/SBA-15, (d) $PtSnAl_{0.3}$/SBA-15, (e) $PtSnAl_{0.4}$/SBA-15.

The TPO profiles of the corresponding catalysts are displayed in Fig. 11. It can be seen that two peaks representing different carbon deposits are displayed in TPO profiles. Generally, the carbon deposits corresponding to the first peak at low temperature are mainly the ones that cover the active metal, while the second peak at high temperature represents the ones that located on the external surface of the support. For PtSnAl/SBA-15 catalysts, it is clear that most of carbon deposits on the support not the active metal. It has been reported by Lieske et al[57] that the presence of Sn not only modifies the electronic properties of the Pt nanoparticles for

promoting the activation of propane but also produces a 'drain-off' effect. This drain-off effect keeps the Pt sites clean by removing the coke precursors from the vicinity of active sites to the support. With increasing of Al content, the maximal peak temperature of TPO profile shifted to higher temperature, which indicates that the degree of the graphitization is getting higher.[58] And this is in accordance with the results of I_D/I_G ratio of Raman. The results of coke analysis indicate that coke is an important factor on the catalysts deactivation, which is demonstrated by the fast deactivation of $PtSnAl_{0.3}$/SBA-15 and $PtSnAl_{0.4}$/SBA-15 with the fast coke formation and large amount of coke.

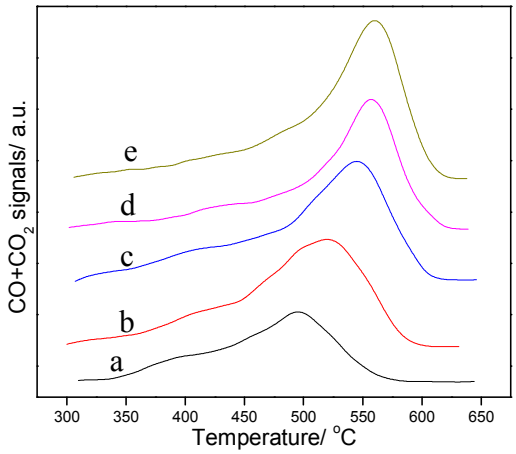

Fig. 11 O_2-TPO curves of the coked catalysts: (a) $PtSnAl_0$/SBA-15, (b) $PtSnAl_{0.1}$/SBA-15, (c) $PtSnAl_{0.2}$/SBA-15, (d) $PtSnAl_{0.3}$/SBA-15, (e) $PtSnAl_{0.4}$/SBA-15.

5 Conclusions

In this work, the PtSnAl/SBA-15 catalysts were synthesized by simultaneous impregnation Al with Pt and Sn precursors. A high activity of propane dehydrogenation has been achieved on $PtSnAl_{0.2}$/SBA-15 with propane conversion 55.9% and propene selectivity 98.5%.

In the PtSnAl/SBA-15 catalyst, most of Al incorporate into the framework of SBA-15 and exist around the metal active centers, which results in the close contact of metal sites and acid sites and favors the synergistic effect for the bifunctional active centers. Moreover, the electron transfer from metal center to the acid center may also happen and lead to the change of the electronic property of Pt, which results in different catalytic performance. The addition of Al can increase the interaction of Sn and support and inhibit the reduction of Sn species during reaction. It consequently improves the propane conversion and catalytic stability.

Furthermore, the addition of Al changes the acidity of the catalysts, which influence the coke formation. In-situ Raman spectra results indicate that the catalysts with different Al contents show different coke formation rate. The excessive addition of Al results in the increase of strong acid, which is favorable for the coke formation and lead to the fast deactivation of the catalyst. The excellent catalytic performance for propane dehydrogenation on $PtSnAl_{0.2}$/SBA-15 catalyst is from the efficient decoration of Pt by interface-confined SnO_x, the confined effect of active centers in mesopores and the best match of noble metal active site and acid site.

Acknowledgements

The authors are grateful for financial support from National Basic Research Program of China (Grant No.2012CB215002), Natural Science Foundation of China (21177160, 21376261, 21303263 and 21173270), Beijing Natural Science Foundation (2142027), Beijing Nova Program (NO. Z141109001814072), Doctor select Foundation (20130007110007, 20130007120011).

Notes and references

[a] *State Key Laboratory of Heavy Oil Processing, China University of Petroleum,18#, Fuxue Road, Chang Ping, Beijing 102249, China. Fax: (+86) 10-89731586(O), E-mail: zhenzhao@cup.edu.cn; liujian@cup.edu.cn.*

[†] *This author contributed equally as the first author.*

Electronic Supplementary Information (ESI) available: [details of any supplementary information available should be included here]. See DOI: 10.1039/b000000x/

1 M. S. Kumar, N. Hammer, M. Rønning, A. Holmen, D. Chen, J. C. Walmsley and G. Øye, *J. Catal.,* 2009, **261**, 116.

2 J. Schäferhans, S. Gómez-Quero, D. V. Andreeva and G. Rothenberg, *Chem. Eur. J.,* 2011, **17**, 12254.

3 J. H. Yun and R. F. Lobo, *J. Catal.,* 2014, **312**, 263.

4 P. Biloen, F. M. Dautzenberg and W. M. H. Sachtler, *J. Catal.,* 1977, **50**, 77.

5 Z. Nawaz, X. P. Tang, Y. Wang and F. Wei, *Ind. Eng. Chem. Res.,* 2010, **49**, 1274.

6 J. J. H. B. Sattler, A. M. Beale and B. M. Weckhuysen, *Phys. Chem. Chem. Phys.,* 2013, **15**, 12095.

7 G. Meitzner, G. H. Via, F. W. Lytle, S. C. Fung and J. H. Sinfelt, *J. Phys. Chem.,* 1988, **92**, 2925.

8 H. Verbeek and W. M. H. Sachtler, *J. Catal.,* 1976, **42**, 257.

9 J. R. Kitchin; J. K. Norskov, M. A. Barteau and J. G. Chen, *Phys. Rev. Lett.,* 2004, **93**, 156801-1.

10 S. B. He, C. L. Sun, Z. W. Bai, X. H. Dai and B. Wang, *Appl Catal A: Gen.,* 2009, **356**, 88.

11 C. L. Yu, Q. J. Ge, H. Y. Xu and W. Z. Li, *Appl Catal A: Gen*., 2006, **315**, 58.

12 Y. W. Zhang, Y. M. Zhou, J. J. Shi, S. J. Zhou, Z. W. Zhang, S. C. Zhang and M. P. Guo, *Fuel process. Technol.,* 2013, **111**, 94.

13 S. Gómez-Quero, T. Tsoufis, P. Rudolf, M. Makkee, F. Kapteijn and G. Rothenberg, *Catal. Sci. Technol.,* 2013, **3**, 962.

14 N. R. Shiju, A. H. Alberts, S. Khalid, D. R. Brown and G. Rothenberg, *Angew. Chem. Int. Ed.,* 2011, **50**, 9615.

15 J. M. Sun and X. H. Bao, *Chem. Eur. J.,* 2008, **14**, 7478.

16 B. K. Vu, S. M. Bok, I. Y. Ahn and E. W. Shin, *Catal. Lett.,* 2009, **133**, 376.

17 S. D. Jackson, G. J. Kelly and G. Web, *J. Catal.,* 1998, **176**, 225.

18 O. A. Bariås, A. Holmen and E. A. Blekkan, *Catal. Today,* 1995, **24**, 361.

19 L. H. Huang, B. L. Xu, L. L. Yang and Y. N. Fan *Catal. Commun.,* 2008, **9**, 2593.

20 Q. Li, Z. J. Sui, X. G. Zhou, Y. Zhu, J. H. Zhou and D. Chen, *Top Catal,.* 2011, **54**, 888.

21 D. Y. Zhao, J. L. Feng, Q. S. Huo, N. Melosh, G. H. Fredrickson, B. F. Chmelka and G. D. Stucky, *Science*, 1998, **279**, 548.

22 A. Ungureanu, B. Dragoi, A. Chirieac, C. Ciotonea, S. Royer, D. Duprez, A. S. Mamede and E. Dumitriu, *ACS Appl. Mater. Interfaces.,* 2013, **5**, 3010.
23 A. K. Medina-Mendoza, M. A. Cortés-Jácome, J. A. Toledo-Antonio, C. Angeles-Chávez, E. López-Salinas, I. Cuauhtémoc-López, M. C. Barrera, J. Escobar, J. Navarrete and I. Hernández, *Appl. Catal. B: Environ.,* 2011, **106**, 14.
24 Z. Kónya, V. F. Puentes, I. Kiricsi, J. Zhu, A. P. Alivisatos and G. A. Somorjai, *Nano Lett.,* 2002, **2**, 907.
25 R. M. Rioux, H. Song, J. D. Hoefelmeyer, P. Yang and G. A. Somerjai, *J. Phys. Chem. B,* 2005, **109**, 2192.
26 M. S. Kumar, A. Holmen and D. Chen, *Microporous Mesoporous Mater.,* 2009, **126**, 152.
27 Z. J. Wang, Y. B. Xie and C. J. Liu, *J. Phys. Chem. C,* 2008, **112**,19818.
28 K. Moller and T. Bein, *Chem. Mater.,* 1998, **10**, 2950–2963.
29 R. Rachwalik, Z. Olejniczak, J. Jiao, J. Huang, M. Hunger and B. Sulikowski, *J. Catal.,* 2007, **252**, 161.
30 W. W. Lonergan, D. G. Vlachos and J. G. Chen, *J. Catal.,* 2010, **271**, 239.
31 A. Shanmugasundaram, P. Basak, L. Satyanarayana and S. V. Manorama, *Sensor. Actuat. B: Chem.,* 2013, **185**, 265.
32 B. K. Vu, M. B. Song, I. Y. Ahn, Y. Suh, D. J. Suh, W. Kim, H. Koh, Y. G. Choi and E. W. Shin, *Appl Catal A: Gen.,* 2011, **400**, 25.
33 J. C. Serrano-Ruiz, G. W. Huber, M. A. Sánchez-Castillo, J. A. Dumesic, F. Rodríguez-Reinoso and A. Sepúlveda-Escribano, *J. Catal*., 2006, **241**, 378.
34 S. N. Coman, V. I. Parvulescu, M. D. Bruyn, D. E. D. Vos and P. A. Jacobs, *J. Catal*., 2002, **206**, 218.
35 X. D. Wang, J. Stöver, V. Zielasek, L. Altmann, K. Thiel, K. Al-Shamery, M. Bäumer, H. Borchert, J. Parisi and J. Kolny-Olesiak, *Langmuir,* 2011, **27**, 11052.
36 X. D. Wang, H. B. Yu, D. Y. Hua and S. H. Zhou, *J. Phys. Chem. C,* 2013, **117**, 7294.
37 M. T. Paffet and R. G. Windham, *Surf. Sci.* 1989, **208**, 34.
38 S. Chen, H. Tsai, W. Chuang, J. Lee, C. Tang, C. Lin and S. Cheng, *J. Phys. Chem. C,* 2009, **113**, 15226.
39 S. Roy, K. Bakhmutsky, E. Mahmoud, R. F. Lobo and R. J. Gorte, *ACS Catal*., 2013, **3,** 573.
40 M. Boronat, P. Concepción, A. Corma, M. Renz and S. Valencia, *J. Catal*., 2005,**234**, 111.
41 F. Bin, C. L. Song, G. Lv, X. F. Cao, H. T. Pang and K. P. Wang, *J Phys Chem C*, 2012, **116**, 26262.
42 K. Wilson, D. J. Adams, G. Rothenberg and J. H. Clark, *J. Mol. Catal. A: Chem.,* 2000, **159**, 309.
43 P. Treesukol, K. Srisuk, J. Limtrakul and T. N. Truong, *J. Phys. Chem. B,* 2005, **109**, 11940.
44 J. A. Rodriguez and J. Hrbek, *Surf. Sci*., 2010, **604**, 241.
45 K. Liu, A. Q. Wang and T. Zhang, *ACS Catal*., 2012, **2**, 1165.
46 Y. W. Zhang, Y. M. Zhou, L. Huang, M. W. Xue and S. B. Zhang, Ind. Eng. *Chem. Res*., 2011, **50**, 7896.
47 M. L. Yang, Y. A. Zhu, X. G. Zhou, Z. J. Sui and D. Chen, *ACS Catal*., 2012, 2, 1247.
48 A. W. Hauser, J. Gomes, M. Bajdich, M. Head-Gordon and A. T. Bell, *Phys. Chem. Chem. Phys.,* 2013, **15**, 20727
49 L. Nykänen and K. Honkala, *ACS Catal*., 2013, **3**, 3026.
50 A. Kuhlmann, F. Roessner, W. Schwieger, O. Gravenhorst and T. Selvam*, Catal. Today,* 2004, **97**, 303.
51 P. B. Weisz and E. W. Swegler, *Science,* 1957, **126**, 31.
52 M. Guisnet and N. S. Gnep, *Catal. Today,* 1996, **31**, 275.
53 C. Li and P. C. Stair, *Catal. Today,* 1997, **33**, 353.
54 I. E. Wachs, *Top. Catal*., 1999, **8**, 57.
55 B. M. Vogelaar, A. Dick van Langeveld, S. Eijsbouts and J. A. Moulijn, *Fuel,* 2007, **86**, 1122.
56 A. Iglesias-Juez, A. M. Beale, K. Maaijen, T. C. Weng, P. Glatzel and B. M. Weckhuysen, *J. Catal*., 2010, **276**, 268.
57 H. Lieske, A. Sárkány and J. Völter, *Appl. Catal.*, 1987, **30**, 69.
58 S. B. He, C. L. Sun, X. Yang, B. Wang, X. H. Dai and Z. W. Bai, *Chem. Eng. J.*, 2010, **163**, 389.